Available online at www.sciencedirect.com

ScienceDirect

Ceramics International 40 (2014) 4077–4083

CERAMICS INTERNATIONAL

www.elsevier.com/locate/ceramint

Phase stability and hot corrosion behavior of ZrO_2–Ta_2O_5 compound in Na_2SO_4–V_2O_5 mixtures at elevated temperatures

M.H. Habibi[a], Shizhong Yang[b], S.M. Guo[a,*]

[a]Dept. of Mechanical and Industrial Engineering, Louisiana State University, Baton Rouge, LA 70803, USA,
[b]LONI Institute/Department of Computer Science, Southern University and A&M College, Baton Rouge, LA 70813, USA

Received 14 July 2013; received in revised form 13 August 2013; accepted 13 August 2013
Available online 22 August 2013

Abstract

For thermal barrier coating (TBC) applications, yttria stabilized zirconia (YSZ) is susceptible to hot corrosion. This paper examines the hot corrosion performance of ZrO_2/Ta_2O_5 compounds. Different compositions of ZrO_2–Ta_2O_5 samples in the presence of molten mixture of $Na_2SO_4+V_2O_5$ at 1100 °C were tested. The compositions were selected to form tetragonal and orthorhombic phases of zirconium-tantalum oxides. Results show that orthorhombic zirconium-tantalum oxide is more stable, both thermally and chemically in $Na_2SO_4+V_2O_5$ media at 1100 °C, and shows a better hot corrosion resistance than the tetragonal phase.

Keywords: C. Hot corrosion; D. Ta_2O_5; D. ZrO_2; E. Thermal barrier coating (TBC)

1. Introduction

Ceramic thermal barrier coatings (TBCs) are widely used as insulation materials in turbine engines to protect hot-section metallic components. The most commonly used TBC top coat material is yttria-stabilized zirconia (YSZ) with a composition of 6–8 wt% (3.5–4.5 mol%) of Y_2O_3 in ZrO_2 [1–6]. Vanadium and sodium are common impurities found in low grade petroleum fuels. Molten sulfate–vanadate deposits resulting from the using of such fuels are extremely corrosive. Hot corrosion degradation due to molten deposits arising from the aggressive combustion environment is one of the major failure mechanisms for TBCs [7–9].

Much efforts have been devoted to improve the phase stability and hot corrosion resistance of YSZ by doping extra metal oxides, for example, different sizes of rare-earth cations [10–12]. A comparative analysis of various stabilizers including MgO, Y_2O_3, Sc_2O_3, In_2O_3, CeO_2, SmO_2, Gd_2O_3 and TiO_2 appeared in [8]. Scandia- and india-stabilized zirconia were found to be more resistant than YSZ to corrosion by vanadia [13–18]. It is understandable that for an oxide whose cation is more acidic than yttrium, such as scandium, it would be thermodynamically less prone to react with acidic oxides. Thus, zirconia stabilized with such oxides would be more resistant to hot corrosion by acidic oxides [8,14,18]. However, the addition of extra trivalent oxides to YSZ generally decreases the cyclic life and erosion resistance due to the decrease in tetragonality and the high affinity for V_2O_5 [8,19,20].

An alternative approach to improve YSZ is the co-doping of yttria with pentavalent oxides such as Ta_2O_5. Ta_2O_5 has a melting point over 1800 °C. On heating it undergoes a phase transformation at 1360 °C which is well above the typical turbine surface temperatures [21]. According to ionic conductivity measurements [22], tantalum ions reside as substitutional defects in the zirconium lattice, annihilating oxygen vacancies generated by yttria. Data in literature indicate defect association between the larger oxide of Y and the smaller oxide of Ta in YSZ. Such defect association should lower the activity and diffusivity in zirconia solid solution thus make this composition more resistant to hot corrosion [18]. Also, according to acid–base Lewis chemical reactions, by virtue of Ta's position in the periodic table, tantalum is more acidic than vanadium. Thus, the ZrO_2–Ta_2O_5 is expected to be substantially more resistant to corrosion by the acidic oxides

*Corresponding author. Tel.: +1 225 578 7619; fax: +1 225 578 5924.
E-mail address: sguo2@lsu.edu (S.M. Guo).

0272-8842/$ - see front matter © 2013 Elsevier Ltd and Techna Group S.r.l. All rights reserved.
http://dx.doi.org/10.1016/j.ceramint.2013.08.062

than ZrO_2–Y_2O_3. According to Raghavan et al. [23] the Y_2O_3–Ta_2O_5 co-doped zirconia is more resilient to the $NaVO_3$ attack. Ta-doped YSZ, which is stable up to 1500 °C and has a low thermal conductivity, has been reported as one prospective TBC [10,20,24].

On the Y_2O_3–Ta_2O_5–ZrO_2 phase diagram at 1500 °C, [24], apart from the tetragonal zirconia phase, formed by equal co-doping of Y_2O_3–Ta_2O_5 into ZrO_2, a stable orthorhombic zirconia phase ($TaZr_{2.75}O_8$) also exists, when ZrO_2 is doped with low level of Y_2O_3 and high level of Ta_2O_5. Previous reports on Y_2O_3–Ta_2O_5 co-doped zirconia systems mainly have a focus on the system stability with equal co-dopants and on the study of associated thermal properties. The investigated compositions generally have a low Ta_2O_5 content of less than 20 wt% [10,18,24,25]. In this paper, we report the hot corrosion behavior of both tetragonal and orthorhombic phase zirconia samples. ZrO_2–Ta_2O_5 composite mixtures (30–70 wt % Ta_2O_5) and YSZ–Ta_2O_5 composite mixtures (70 wt% YSZ + 30 wt% Ta_2O_5, 30TaYSZ) were made. The hot corrosion behavior of the samples with two different phases in $Na_2SO_4 + V_2O_5$ at 1100 °C is presented.

2. Experimental procedure

Hot corrosion studies using Na_2SO_4 and V_2O_5 mixtures were conducted on samples at 1100 °C in air. For the above mixtures, 95% Na_2SO_4 and 99.9% V_2O_5 from Sigma-Aldrich were used. Five types of ceramic samples, YSZ, 70 wt% ZrO_2 + 30 wt% Ta_2O_5 (30TaSZ), 70 wt% YSZ + 30 wt% Ta_2O_5 (30TaYSZ), 50 wt% ZrO_2 + 50 wt% Ta_2O_5 (50TaSZ), and 30 wt% ZrO_2 + 70 wt% Ta_2O_5 (70TaSZ) were made using agglomerated powders from Sigma-Aldrich. To obtain the samples, powders were first pressed with binders in a uniaxial die (2.5 cm inner diameter) at 350 MPa pressure to obtain the compressed green bodies, which were then sintered at 1450 °C for 5 h and 30 min to obtain the dense bodies. To perform an accelerated high-temperature hot corrosion test on samples, a mixture of 50 wt% Na_2SO_4 + 50 wt% V_2O_5 deposit was spread evenly onto the surfaces of the specimens with a mixed salt amount of 20 mg/cm^2. The specimens were then set in an electric furnace with an ambient atmosphere under a maximum temperature of 1100 °C for 4 h. The furnace has two small holes for air to flow naturally. After each 4 h of testing at 1100 °C, the samples were allowed to cool down inside the furnace, and then the samples were inspected both visually and with an optical microscope for possible crack initiation. To repeat the test, the samples were recoated with the $Na_2SO_4 + V_2O_5$ salt mixture and the heating profile was repeated. The morphology and microstructure of the as received samples and the samples after the hot corrosion tests were examined using field emission scanning electron microscopy (Quanta3D FEG, FEI Company, USA). For surface morphology studies using SEM, a thin Pt layer was sputtered onto the samples to improve the electrical conductivity. X-ray diffraction (MiniFlex XRD, Rigaku Corporation, Japan) with Cu Kα radiation λ=1.54178 Å at a scan speed of 1 deg/min was used to establish the phase composition of the specimen.

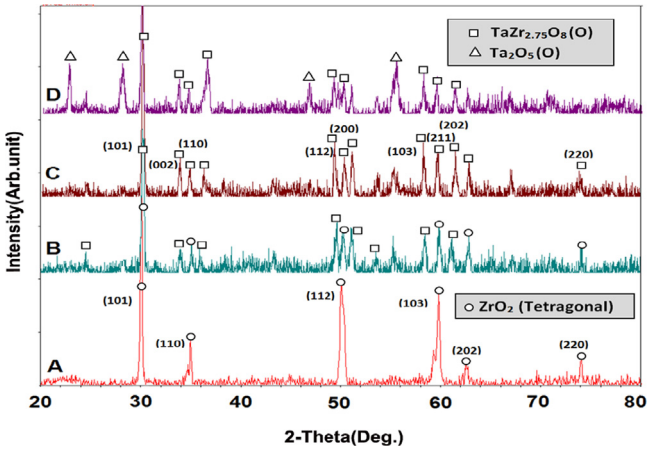

Fig. 1. XRD patterns of as-received (A) YSZ, (B) 30TaSZ, (C) 50TaSZ and (D) 70TaSZ.

3. Results

Fig. 1 depicts the X-ray diffraction patterns for the as-received YSZ, 30TaSZ, 50TaSZ and 70TaSZ specimens. In Fig. 1A, for sintered YSZ, only diffraction peaks corresponding to tetragonal ZrO_2 can be distinguished. In the 30TaSZ, a mixed tetragonal and orthorhombic phases form, and 50TaSZ sample shows a near pure orthorhombic phase of zirconium tantalum oxide. The zirconium tantalum compound in orthorhombic phase is found to be $TaZr_{2.75}O_8$, based on the XRD patterns of 30TaSZ and 50TaSZ. For 70TaSZ sample, besides $TaZr_{2.75}O_8$, well-defined peaks corresponding to Ta_2O_5 are also observed. Note in Fig. 1, the more intense peaks of Ta_2O_5 are at $2\theta = 22.8^\circ$ and 28.3°.

Fig. 2 shows the as-received SEM image of YSZ, 30TaSZ, 50TaSZ and 70TaSZ. These SEM images show a typical microstructure of pressed and sintered samples with certain amount of porosity, visible on the surface of samples. In Fig. 2D, for 70TaSZ sample, there are two distinct microstructures, a matrix of orthorhombic $TaZr_{2.75}O_8$ and some isolated Ta_2O_5 regions. This sample is made of 30 wt% of ZrO_2 mixed with 70 wt% of Ta_2O_5.

Fig. 3 illustrates XRD patterns of YSZ, 30TaSZ, 50TaSZ and 70TaSZ specimens after hot corrosion at 1100 °C in $Na_2SO_4 + V_2O_5$ salt for 40 h (10 cycles). In Fig. 3A, starting from tetragonal phase, after 40 h of tests, a large portion of the YSZ sample changed to the monoclinic phase by the $Na_2SO_4 + V_2O_5$ salt. YVO_4 is formed as the major hot corrosion product.

An examination of XRD pattern of the 30TaSZ sample, besides $TaZr_{2.75}O_8$ and tetragonal zirconia peaks which are present in the original as-received sample, after hot corrosion, some new peaks are identified which can be contributed to monoclinic zirconia, $TaVO_5$ and Ta_9VO_{25}.

SEM images of the YSZ, 30TaSZ, 50TaSZ and 70TaSZ specimens after hot corrosion tests are presented in Fig. 4. Apart from XRD analysis (Fig. 3), Energy Dispersive Spectroscopy (EDS) analysis was performed at different regions of the samples to confirm the chemical compositions of the hot

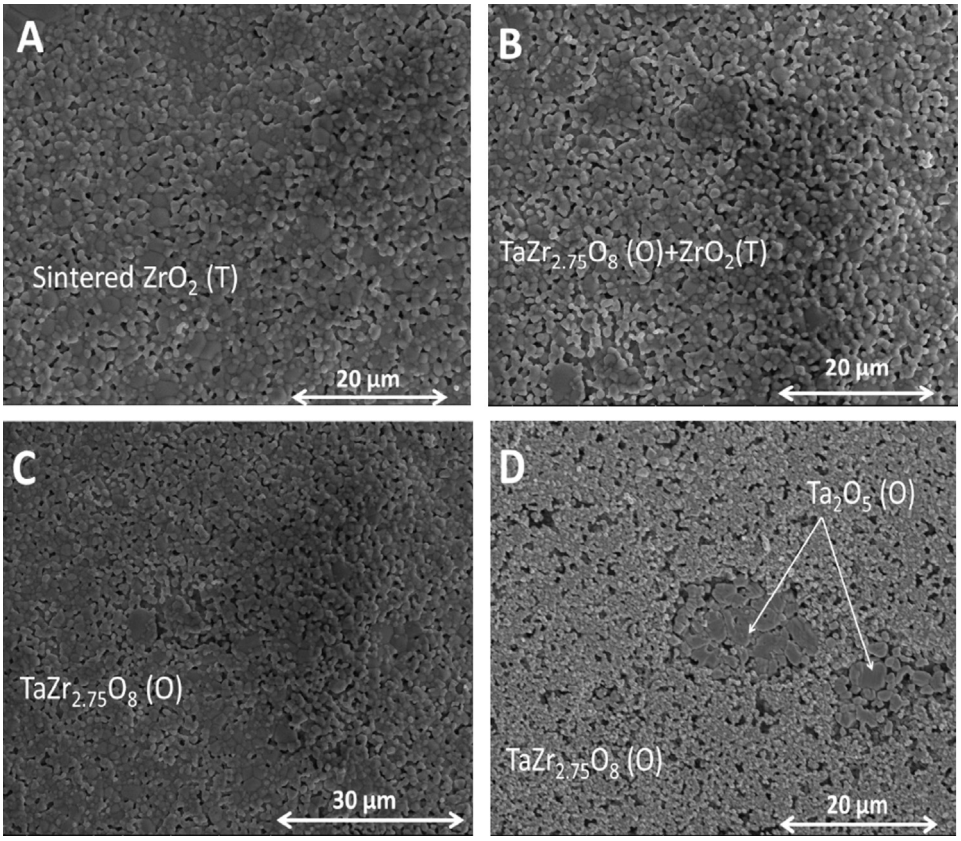

Fig. 2. SEM images of as-received sintered (A) YSZ, (B) 30TaSZ, (C) 50TaSZ and (D) 70TaSZ.

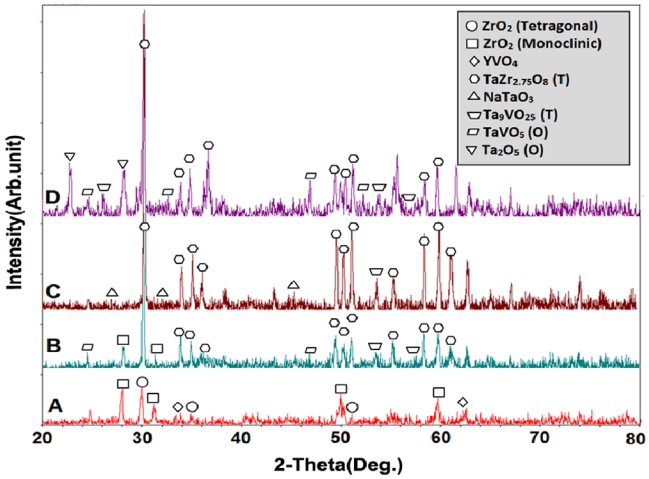

Fig. 3. XRD patterns of (A) YSZ, (B) 30TaSZ, (C) 50TaSZ and (D) 70TaSZ after hot corrosion in $Na_2SO_4+V_2O_5$ at 1100 °C for 40 h.

corrosion products. For crystals in Fig. 4A, EDS analysis demonstrated that these crystals were composed of yttrium, vanadium, and oxygen. Further analysis confirmed these crystals were YVO_4. Hot corrosion products of 30TaSZ sample are rod-shape. The extent of the attack is, however, much smaller in comparison to the YSZ sample.

In the 50TaSZ case, after hot corrosion, only a small quantity of rod-shaped crystals was formed. According to EDS result, crystals in Fig. 4C contain sodium, tantalum and oxygen and with considering the XRD pattern, they are found to be $NaTaO_3$. Most of the $TaZr_{2.75}O_8$ surface did not react with molten salt and it is almost perfectly intact. XRD shows strong peaks of orthorhombic phase of zirconium tantalum oxide.

In 70TaSZ sample, besides TaV_9O_{25}, strong peaks contributed to pure Ta_2O_5 and $TaVO_5$ were also detected, Fig. 3D. The formation of considerable amount of $TaVO_5$ and Ta_9VO_{25} crystals in this sample is due to the large amount of excess Ta_2O_5, which reacts with the molten salt. Considering the intensity of the XRD peaks and the amount of hot corrosion products, reaction rate of 70TaSZ is higher than the 50TaSZ case. However, exposure to $Na_2SO_4+V_2O_5$ salt does not cause destabilization of zirconium tantalum oxide to monoclinic phase seen for the YSZ sample.

It is noteworthy to compare the hot corrosion behavior of 30TaYSZ (30 wt% Ta_2O_5+70 wt% YSZ) with 30TaSZ (30 wt % Ta_2O_5+70 wt% ZrO_2). Fig. 5 shows the XRD patterns of the as-received 30TaYSZ and 30TaSZ. As indicated by the XRD patterns, 30TaYSZ is a pure tetragonal zirconia phase while 30TaSZ is a mixture of tetragonal zirconia and orthorhombic tantalum zirconium oxide ($TaZr_{2.75}O_8$). For 30TaYSZ, the amount of Ta_2O_5 added into YSZ is not high enough to form complex tantalum zirconium oxide. Instead, tetragonal zirconia is found to be the only phase formed, with Ta_2O_5–Y_2O_3 dopants in the ZrO_2 matrix. Similar findings are reported in previous studies [25–27].

Fig. 6 shows XRD patterns of 30TaYSZ and 30TaSZ specimens after hot corrosion at 1100 °C in $Na_2SO_4+V_2O_5$

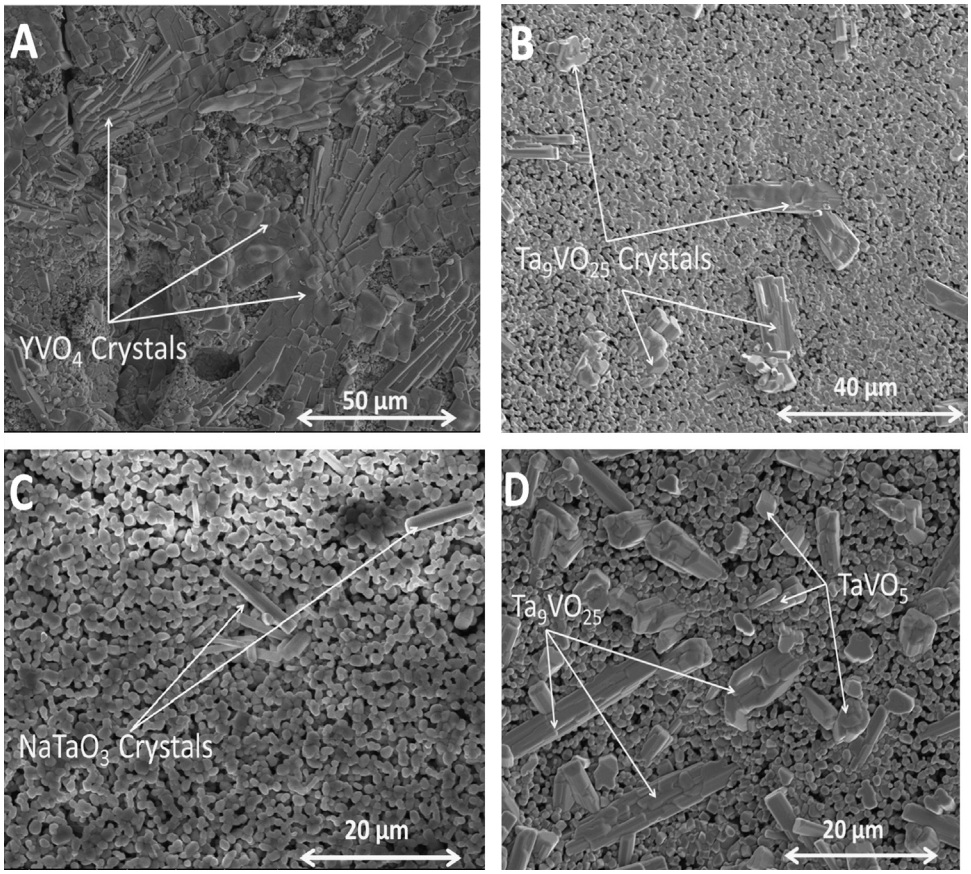

Fig. 4. SEM surface images of (A) YSZ, (B) 30TaSZ, (C) 50TaSZ, and (D) 70TaSZ after hot corrosion in $Na_2SO_4+V_2O_5$ at 1100 °C for 40 h.

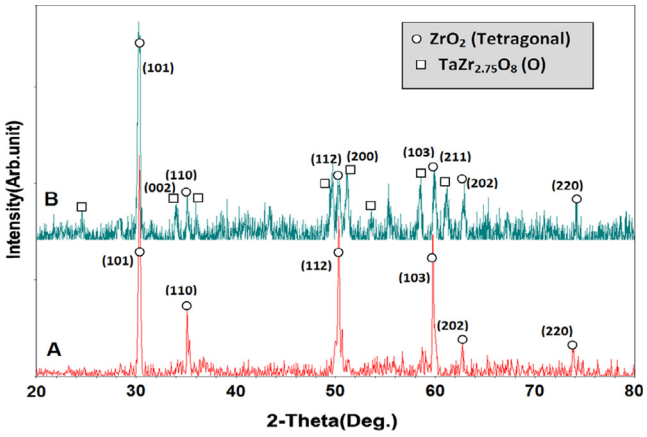

Fig. 5. XRD patterns of as-received (A) 30TaYSZ and(B) 30TaSZ.

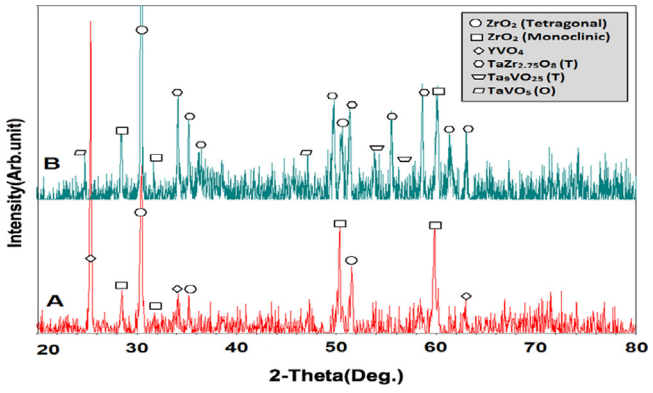

Fig. 6. XRD patterns of (A) 30TaYSZ and (B) 30TaSZ after hot corrosion in $Na_2SO_4+V_2O_5$ at 1100 °C for 40 h.

salt for 40 h. In Fig. 6A, it is seen that the 30TaYSZ sample, which is pure tetragonal to begin with, has high level of monoclinic phase, in conjunction with the formation of YVO_4, due to $Na_2SO_4+V_2O_5$ salt corrosion. Besides orthorhombic $TaZr_{2.75}O_8$ and tetragonal zirconia, some new peaks are identified on 30TaSZ sample after hot corrosion, which are monoclinic zirconia, $TaVO_5$ and Ta_9VO_{25}. Fig. 7 shows SEM images of 30TaYSZ and 30TaSZ after hot corrosion at 1100 °C in $Na_2SO_4+V_2O_5$ salt for 40 h. Based on the quantity of corrosion products, 30TaSZ is found to have a better hot corrosion resistance than 30TaYSZ, due to the formation of the highly stable orthorhombic $TaZr_{2.75}O_8$ phase.

4. Discussion

For a conventional Y_2O_3-stabilized ZrO_2, a Na_2SO_4–V_2O_5 mixture can leach out Y_2O_3 as follows [3,13,28,29]. $NaVO_3$ forms due to the presence of both V_2O_5 and Na_2SO_4

$$V_2O_5+Na_2SO_4 \rightarrow 2(NaVO_3)+SO_3 \quad (1)$$

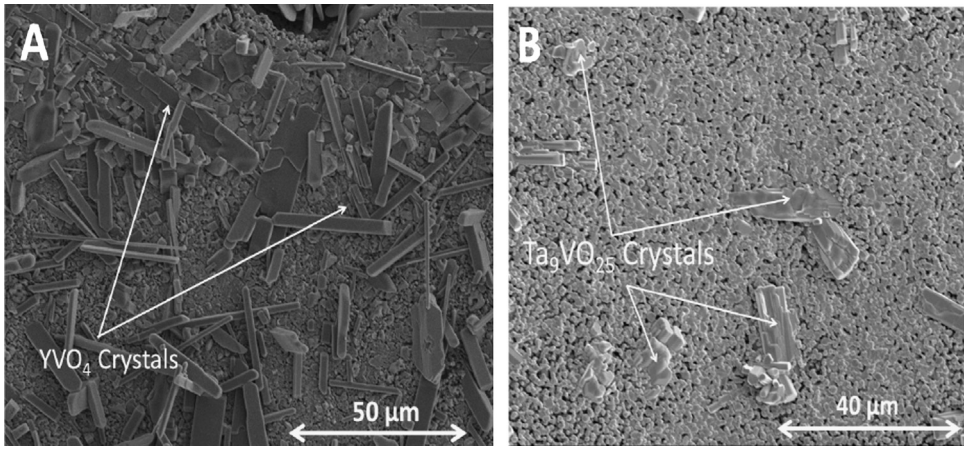

Fig. 7. SEM surface images of (A) 30TaYSZ and (B) 30TaSZ, after hot corrosion in $Na_2SO_4+V_2O_5$ at 1100 °C for 40 h.

Table 1
At 1500 K, Gibbs free energy of formation in unit kJ/mol.

Substance	Y_2O_3	$NaVO_3$	YVO_4	Na_2O	Ta_2O_5	$NaTaO_3$	$TaVO_5$	Ta_9VO_{25}
Gibbs energy	−2713.24	−1501.93	−3960.34	−494.51	−1719.71	−1304.14	−2048.53	−10693.86

The Gibbs free energy of formation for this reaction is [30,34]

$$\Delta G^0_{298\ K} = \Sigma\Delta G^0_{products} - \Sigma\Delta G^0_{reactants} = -2087.845\ kJ/mol$$

$$\Delta G^0_{1400\ K} = -1686.066\ kJ/mol$$

Then, $NaVO_3$, having a melting point of 610 °C, reacts with yttria from the YSZ solid solution to form YVO_4

$$ZrO_2(Y_2O_3)+2(NaVO_3)\rightarrow ZrO_2+2(YVO_4)+Na_2O \quad (2)$$

Na_2O released by above reaction can form more $NaVO_3$. Na_2O can react with V_2O_5 directly to form $NaVO_3$

$$Na_2O\ (base)+V_2O_5\ (acid)\rightarrow 2NaVO_3\ (salt) \quad (3)$$

The molten $NaVO_3$ is also reported to increase mobility of Y^{3+}, hence further promotes the depletion of yttria from YSZ and the growth of YVO_4 crystals. After losing Y_2O_3, the transformation of tetragonal zirconia to monoclinic zirconia during the cooling stage of thermal cycling is accompanied by a 3–5% volume expansion, leading to cracking and spallation of the YSZ coating.

For 30TaSZ, 50TaSZ and 70TaSZ, as described earlier, Na_2SO_4 and V_2O_5 would first react and form $NaVO_3$, then, the possible reactions that would have produced those identified reaction products include [8,18,20]

$$TaSZ(Ta_2O_5)\ (s)+NaVO_3\ (l)\rightarrow NaTaO_3\ (s)+TaVO_5\ (s) \quad (4)$$

$$TaSZ(5Ta_2O_5)\ (s)+NaVO_3\ (l)\rightarrow NaTaO_3\ (s)+Ta_9VO_{25}\ (s) \quad (5)$$

In this study, there are many unusual substances, such as $TaVO_5$ and Ta_9VO_{25}, whose thermodynamic data cannot be found easily. The authors checked several common handbooks, databases and software packages, such as the CRC Handbook of Chemistry and Physics, the Bureau of Mines and USGS database, the NIST-JANAF Thermochemical Tables, the MatNavi NIMS Materials Database, the HSC Chemistry package, etc. and failed to obtain useful information. A literature search also failed to generate the required complete thermodynamic data set [8,30–36]. To further assist the understanding of the corrosive reactions, the authors performed the *ab initio* density functional theory (DFT) based electronic structure simulations to obtain the relevant thermodynamic data. The Gibbs free energy of formation was calculated for each reactant and product by summation of the energy formation at 0 K, zero point energy, vibrational internal energy and free energy at 1227 °C, and PV term. The phonon module in the software MedeA [37] was used to calculate the thermodynamic vibration parameters. The (VASP) [37–40] was used to perform DFT calculations where plane wave basis set was implemented. The *ab initio* projector augmented wave (PAW) [41–42] general gradient approximation (GGA) calculation method with plane wave basis sets was used and 400 eV plane wave cut-off energy was set in the simulation. Each lattice in all of the supercells was selected to be larger than ~7 Å. Only harmonic vibration approximation was considered in the phonon calculations. The calculated Gibbs free energy of formation results are shown in Table 1.

For $NaTaO_3$, the Gibbs free energy of formation at 1500 K is −1304.14 kJ/mol, while the Gibbs free energy of formation for $TaVO_5$ at 1500 K is −2048.53 kJ/mol. To make a comparison, the Gibbs free energy of formation of YVO_4 at 1500 K is −3960.34 kJ/mol. So, YVO_4 (Eq. (2)) is much more stable than both $NaTaO_3$ and $TaVO_5$ (Eqs. (4) and (5)). Based on the calculated Gibbs free energy results, Eq. (2) is found to be endothermic while Eqs. (4) and (5) are exothermic reactions. However, in Eq. (2), since Na_2O has a low melting temperature of 1132 °C, Y_2O_3 and YVO_4 can be easily dissolved in Na_2O. Also Na_2O can further feed the formation

of $NaVO_3$ through Eq. (3). All these explain the experimentally observed fast reaction of Eq. (2) than Eqs. (4) and (5).

V_2O_5 may also react with Ta_2O_5 directly at elevated temperature. According to Ta_2O_5–V_2O_5 phase diagram, in temperatures lower than 1200 °C, two possible components are $TaVO_5$ and Ta_9VO_{25} [8,43].

$$V_2O_5\ (l) + TaSZ(Ta_2O_5)\ (s) \rightarrow 2TaVO_5\ (s) \quad (6)$$

$$V_2O_5\ (l) + 9TaSZ(Ta_2O_5)\ (s) \rightarrow 2Ta_9VO_{25}\ (s) \quad (7)$$

The detection of orthorhombic $TaZr_{2.75}O_8$ by XRD and EDS over a vast surface area of the 50TaSZ sample after hot corrosion suggests that this orthorhombic phase is stable to the molten salt attack. Molten salt is found to react with both Y_2O_3 and Ta_2O_5. Y^{3+} in the lattice of ZrO_2 has the mobility to migrate preferentially toward the reaction interface due to the high V concentration present on the sample surfaces [28]. The reactions between vanadium compounds and ceramic oxides follow a Lewis acid–base mechanism, where the acid vanadium compounds react more readily with the ceramic oxides that have stronger basicity. As reported in literature, the basicity of tantalum oxide, yttrium oxide, and zirconium dioxide follows the order: $Y_2O_3 > Ta_2O_5 > ZrO_2$, indicating that molten $NaVO_3$ has the tendency to react with Y_2O_3 more easily [7,8,29]. Following the nucleation and growth mechanism, at the beginning of the hot corrosion process, the hot corrosion products ($TaVO_5$, Ta_9VO_{25} and YVO_4) have dendritic like shapes; then as the hot corrosion proceeds, these hot corrosion products become larger and their morphologies change to rod/plate-like shapes. Based on thermodynamic data and basicity of Y_2O_3 and Ta_2O_5 and their tendency to react with molten salt, the growth rate of $TaVO_5$ and Ta_9VO_{25} is slower than that of YVO_4 in the prolonged hot corrosion tests which indicate better stability of zirconia, stabilized with Ta_2O_5 rather than with Y_2O_3.

Comparing all samples tested in this study, hot corrosion resistance of 50TaSZ is the best. This sample has a near single orthorhombic phase of $TaZr_{2.75}O_8$, which is highly stable in high temperatures and resistant to hot corrosion attack in molten salts.

5. Conclusions

The hot corrosion resistances of different compositions of YSZ, ZrO_2, and Ta_2O_5 samples to $Na_2SO_4 + V_2O_5$ mixture were studied, under a typical gas turbine component surface temperature of 1100 °C. The samples were selected to form both tetragonal and orthorhombic zirconium-tantalum oxides. Results show that orthorhombic zirconium-tantalum oxide is more stable, both thermally and chemically in $Na_2SO_4 + V_2O_5$ media at 1100 °C, and shows a better hot corrosion resistance than the tetragonal phase. Thus orthorhombic zirconium-tantalum oxides offer good opportunities for developing novel TBCs with improved resistance to corrosion by sulfate/vanadate melts.

Disclaimer

Acknowledgments

This publication is based upon work supported by the US Department of Energy National Energy Technology Laboratory under Award no. DE-FE0004734 and NASA-EPSCoR Program (Grant NNX09AP72A).

References

[1] L. Wang, Y. Wang, X.G. Sun, J.Q. He, Z.Y. Pan, C.H. Wang, Thermal shock behavior of 8YSZ and double-ceramic-layer $La_2Zr_2O_7$/8YSZ thermal barrier coatings fabricated by atmospheric plasma spraying, Ceramics International 38 (2012) 3595–3606.

[2] C.S. Ramachandran, V. Balasubramanian, P.V. Ananthapadmanabhan, Synthesis, spheroidization and spray deposition of lanthanum zirconate using thermal plasma process, Surface and Coatings Technology 206 (2012) 3017–3035.

[3] R. Ahmadi-Pidani, R. Shoja-Razavi, R. Mozafarinia, H. Jamali, Evaluation of hot corrosion behavior of plasma sprayed ceria and yttria stabilized zirconia thermal barrier coatings in the presence of $Na_2SO_4 + V_2O_5$ molten salt, Ceramics International 38 (2012) 6613–6620.

[4] S. Yugeswaran, V. Selvarajan, M. Vijay, P.V. Ananthapadmanabhan, K.P. Sreekumar, Influence of critical plasma spraying parameter (CPSP) on plasma sprayed alumina–titania composite coatings, Ceramics International 36 (2010) 141–149.

[5] M. Fritsch, H. Klemm, M. Herrmann, B. Schenk, Corrosion of selected ceramic materials in hot gas environment, Journal of the European Ceramic Society 26 (2006) 3557–3565.

[6] C.S. Ramachandran, V. Balasubramanian, P.V. Ananthapadmanabhan, Thermal cycling behaviour of plasma sprayed lanthanum zirconate based coatings under concurrent infiltration by a molten glass concoction, Ceramics International 39 (2013) 1413–1431.

[7] R.L. Jones, Some aspects of the hot corrosion of thermal barrier coatings, Journal of Thermal Spray Technology 6 (1997) 77–84.

[8] R.L. Jones, Vanadate-Sulfate Melt Thermochemistry Relating to Hot Corrosion of Thermal Barrier Coatings, Naval Research Laboratory, 1997, pp. 1–10.

[9] J. Xiang, S. Chen, J. Huang, H. Zhang, X. Zhao, Phase structure and thermophysical properties of co-doped $La_2Zr_2O_7$ ceramics for thermal barrier coatings, Ceramics International 38 (2012) 3607–3612.

[10] A. Bhattachaya, V. Shklover, K. Kunze, W. Steurer, Effect of 7YSZ on the long-term stability of $YTaO_4$ doped ZrO_2 system, Journal of the European Ceramic Society 31 (2011) 2897–2901.

[11] B.S.Uwe Schulz, Klaus Fritscher, Christoph Leyens, Review on advanced EB-PVD ceramic topcoats for TBC applications, International Journal of Applied Ceramic Technology 1 (2004) 302–315.
[12] G. Di Girolamo, C. Blasi, M. Schioppa, L. Tapfer, Structure and thermal properties of heat treated plasma sprayed ceria–yttria co-stabilized zirconia coatings, Ceramics International 36 (2010) 961–968.
[13] P. Mohan, B. Yuan, T. Patterson, V.H. Desai, Y.H. Sohn, Degradation of yttria-stabilized zirconia thermal barrier coatings by vanadium pentoxide, phosphorous pentoxide, and sodium sulfate, Journal of the American Ceramic Society 90 (2007) 3601–3607.
[14] M.H. Habibi, L. Wang, S. Guo, An investigation on hot corrosion resistance of plasma sprayed composite YSZ–$Gd_2Zr_2O_7$ and $Gd_2Zr_2O_7$ thermal barrier coayings in simulated turbine environment at 1050 °C, in: Proceedings of the 12th ASME 2012 International Mechanical Engineering Congress, ASME, Houston,Texas, 2012.
[15] S.Y. Park, J.H. Kim, M.C. Kim, H.S. Song, C.G. Park, Microscopic observation of degradation behavior in yttria and ceria stabilized zirconia thermal barrier coatings under hot corrosion, Surface and Coatings Technology 190 (2005) 357–365.
[16] Z. Chen, J. Mabon, J.-G. Wen, R. Trice, Degradation of plasma-sprayed yttria-stabilized zirconia coatings via ingress of vanadium oxide, Journal of the European Ceramic Society 29 (2009) 1647–1656.
[17] M. Saremi, M.H. Habibi, An investigation on hot corrosion resistance of plasma sprayed YSZ–Ceria TBC in Na_2SO_4+V_2O_5 at 1050 °C, in: TMS 2011 – 140th Annual Meeting and Exhibition, Supplemental Proceedings, John Wiley & Sons, Inc., 2011, pp. 429–437.
[18] S. Raghavan, J. Mayo, The hot corrosion resistance of 20 mol% $YTaO_4$ stabilized tetragonal zirconia and 14 mol% Ta_2O_5 stabilized orthorhombic zirconia for thermal barrier coating applications, Surface and Coatings Technology 160 (2002) 187–196.
[19] J.R. Brandon, R. Taylor, Thermal properties of ceria and yttria partially stabilized zirconia thermal barrier coatings, Surface and Coatings Technology 39–40 (Part 1) (1989) 143–151.
[20] F.M. Pitek, C.G. Levi, Opportunities for TBCs in the ZrO_2–$YO_{1.5}$–$TaO_{2.5}$ system, Surface and Coatings Technology 201 (2007) 6044–6050.
[21] M. Moldovan, C.M. Weyant, D.L. Johnson, K.T. Faber, Tantalum oxide coatings as candidate environmental barriers, Journal of Thermal Spray Technology 13 (2004) 51–56.
[22] S. Raghavan, W.D. Porter, R.B. Dinwiddie, M.J. Mayo, Thermal properties of zirconia co-doped with trivalent and pentavalent oxides, Acta Materialia 49 (2001) 169–179.
[23] H.W.Srinivasan Raghavan, Ralph B. Dinwiddie, Wallace D. Porter, Robert Vaben, Detlev Stover, Merrilea J. Mayo, Ta_2O_5/Nb_2O_5 and Y_2O_3 co-doped zirconias for thermal barrier coatings, Journal of the American Ceramic Society 87 (2004) 431–437.
[24] Y. Shen, R.M. Leckie, C.G. Levi, D.R. Clarke, Low thermal conductivity without oxygen vacancies in equimolar $YO_{1.5}$+$TaO_{2.5}$- and $YbO_{1.5}$+$TaO_{2.5}$-stabilized tetragonal zirconia ceramics, Acta Materialia 58 (2010) 4424–4431.
[25] A.K. Bhattacharya, V. Shklover, W. Steurer, G. Witz, H.-p. Bossmann, O. Fabrichnaya, Ta_2O_5–Y_2O_3–ZrO_2 system: experimental study and preliminary thermodynamic description, Journal of the European Ceramic Society 31 (2011) 249–257.
[26] G. Gritzner, C. Puchner, V_2O_5, Nb_2O_5 and Ta_2O_5 doped zirconia ceramics, Journal of the European Ceramic Society 13 (1994) 387–394.
[27] T. Tien, D.J. Kim, Phase stability and physical properties of cubic and tetragonal ZrO_2 in the system ZrO_2–Y_2O_3–Ta_2O_5, Journal of the American Ceramic Society 74 (1991) 3061–3065.
[28] W. Hertl, Vanadia reaction with yttria stabilized zirconia, Journal of Applied Physics 63 (1988) 5514–5520.
[29] M.H. Habibi, L. Wang, S.M. Guo, Evolution of hot corrosion resistance of YSZ, $Gd_2Zr_2O_7$, and $Gd_2Zr_2O_7$+YSZ composite thermal barrier coatings in Na_2SO_4+V_2O_5 at 1050 °C, Journal of the European Ceramic Society 32 (2012) 1635–1642.
[30] NIST-JANAF Thermochemical Tables, ⟨http://kinetics.nist.gov/janaf/⟩.
[31] K.L. Luthra, H.S. Spacil, Impurity deposits in gas turbines from fuels coating sodium and vanadium, Journal of the Electrochemical Society: Solid-State Science and Technology (1982) 649–656.
[32] H. Yokokawa, N. Sakai, T. Kawada, M. Dokiya, Chemical potential diagrams for rare earth-transition metal-oxygen systems: Ln–V–O and Ln–Mn–O systems, Journal of the American Ceramic Society 73 (3) (1990) 649–658.
[33] Alla D. Mah, Thermodynamic Properties of Vanadium and its Compounds, Report of Investigations/United States Department of the Interior, Bureau of Mines, Number 6727, 1966.
[34] I. Barin, O. Knacke, O. Kubaschewski, Thermochemical Properties of Inorganic Substances, 1st edition, Springer-Verlag, Berlin, New York, 1973.
[35] Woo Y. Lee, Yong W. Bae, Na_2SO_4-Induced corrosion of Si_3N_4 coated with chemically vapor deposited Ta_2O_5, Journal of the American Ceramic Society 78 (7) (1995) 1927–1930.
[36] J. Hinden, J. Augustynski, Etude des systems Na_3AlF_6–Ta_2O_5 ET Na_3AlF_6–$NaTaO_3$, Electrochimica Acta 20 (1975) 629–633.
[37] G. Kresse, J. Hafner, *Ab initio* molecular dynamics for liquid metals, Physical Review B 47 (1993) 558–561.
[38] G. Kresse, J. Furthmüller, Efficiency of *ab-initio* total energy calculations for metals and semiconductors using a plane-wave basis set, Computational Materials Science 6 (1996) 15–50.
[39] G. Kresse, J. Furthmüller, Efficient iterative schemes for *ab initio* total-energy calculations using a plane-wave basis set, Physical Review B 54 (1996) 11169–11186.
[40] VASP 2013 manual. Available from: http://cms.mpi.univie.ac.at/vasp/.
[41] P.E. Blöchl, Projector augmented-wave method, Physical Review B 50 (1994) 17953–17979.
[42] G. Kresse, D. Joubert, From ultrasoft pseudopotentials to the projector augmented-wave method, Physical Review B 59 (1999) 1758–1775.
[43] H. Schadow, H. Wehner, Investigations on the quasi-binary system V_2O_5–Ta_2O_5, Crystal Research and Technology 27 (1992) 691–695.